

# Comparison of Human and Bovine Insulin Amyloidogenesis under Uniform Shear

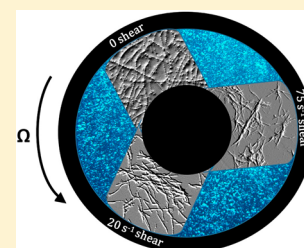
Samantha A. McBride,<sup>†</sup> Christopher F. Tilger,<sup>‡</sup> Sean P. Sanford,<sup>§</sup> Peter M. Tessier,<sup>†</sup> and Amir H. Hirs<sup>\*,†,‡</sup>

<sup>†</sup>Department of Chemical and Biological Engineering, <sup>‡</sup>Department of Mechanical, Aerospace, and Nuclear Engineering, and

<sup>§</sup>Department of Biomedical Engineering, Rensselaer Polytechnic Institute, 110 Eighth Street, Troy, New York 12180, United States

## Supporting Information

**ABSTRACT:** A diverse range of proteins can assemble into amyloid fibrils, a process that generally results in a loss of function and an increase in toxicity. The occurrence and rate of conversion is strongly dependent on several factors including molecular structure and exposure to hydrodynamic forces. To investigate the origins of shear-induced enhancement in the rate of fibrillization, a stable rotating Couette flow was used to evaluate the kinetics of amyloid formation under uniform shear for two similar insulin species (human and bovine) that demonstrate unique fibrillization kinetics. The presence of shear-induced nuclei predicted by previous studies is supported by observations of a lag between the consumption of soluble insulin and the precipitation of amyloid aggregates. The apparent fibrillization rate generally increases with shear. However, a two-parameter kinetic model revealed that the nucleation rate has a maximum value at intermediate shear rates. The fibril elongation rate increases monotonically with shear and is similar for both insulin variants, suggesting that increased elongation rates are related to mixing. Differences between human and bovine insulin kinetics under shear are attributable to the nucleation step.



## INTRODUCTION

The link between protein misfolding and assembly into amyloid fibrils and numerous neurodegenerative diseases has motivated the investigation of amyloid assembly pathways.<sup>1,2</sup> Amyloid fibrils are long, crystalline structures that assemble from many polypeptide monomers combining in a templated fashion into thin fibers. The generic mechanism for fibril formation is as follows: (i) protein conformational change or assembly into a fibril nucleus, (ii) proto-fibril elongation driven by the interaction of protein monomers with nuclei, and (iii) proto-fibrils intertwining into mature fibrils.<sup>2,3</sup> Amyloid fibril formation is difficult to quantify because of the large variety of proteins of different shapes, sizes and functions that undergo amyloidogenesis to form fibrils. Many different proteins are known to fibrillize despite large differences in their structure and sequence.<sup>2</sup> Adding to this complication is the influence of several factors on fibril formation. Ionic strength, pressure, and temperature, as well as hydrodynamic forces and extreme pH values, have been shown to modulate the rate of amyloid formation for diverse proteins.<sup>2,3</sup>

Numerous agitation studies have demonstrated that fibrillization increases with increased fluid flow, yet the mechanism responsible for this deleterious effect on protein stability remains unclear.<sup>4–17</sup> One proposed mechanism suggests that the increase in fibrillization with shear occurs because protein molecules are stretched and deformed when placed in an extensional flow field.<sup>5–7</sup> The initial deformation exposes buried hydrophobic residues such that a nucleation site can form. This hypothesis is supported by the observation that the increase in nucleation rate occurs at the onset of shear for some types of protein.<sup>8,9</sup> Similar extensional-deformation mecha-

nisms have been reported for unfolding of polymers within a shear field.<sup>10</sup> In the case of proteins, however, the monomers are often small enough that the extensional force on individual molecules from tip to tip is negligible. Molecular dynamic simulations and simple calculations suggest that the shear force required to induce protein unfolding is much larger than the forces that have been experimentally shown to result in increased fibrillization.<sup>9,11</sup> On the basis of this observation, it has been suggested that the influence of shear is instead to align the protein monomers and promote intermolecular interactions.<sup>5,9,12</sup>

Alternative explanations for the shear effect on fibrillization kinetics reject the notion that shear influences protein structure or molecular alignment. The simplest of these explanations posits that shearing flows act by increasing the degree of mixing such that reaction rates are no longer diffusion limited.<sup>13</sup> The mixing hypothesis has been rejected by some reports.<sup>14,15</sup> Other factors, namely the air–water interface that often accompanies agitation, may also contribute to the effects of shear on fibrillization kinetics.<sup>15–17</sup> The lack of consensus regarding the mechanism warrants further investigation into the hydrodynamics and role of shear in amyloid fibril formation.

To investigate whether increased fibrillization kinetics under flow are the simple result of increased mixing or due to other shear-induced effects, it is necessary to perform experiments in a uniform shear field. However, imposition of a uniform shear field can be difficult to achieve under laboratory conditions.

Received: May 10, 2015

Revised: July 23, 2015

Published: July 30, 2015

The flat-plate geometry of Couette in which fluid is contained between two infinite plates (one moving at a fixed velocity, the other stationary) yields uniform shear.<sup>18</sup> In practice, concentric cylinder devices are used to imitate this ideal scenario in a cylindrical system. Fluid is placed in a small gap between two concentric cylinders, and one cylinder is rotated while the other remains stationary. This geometry is known as either “Couette” or “Taylor-Couette.” Rotation of the inner cylinder is common because outer cylinder rotation generally requires a more complicated apparatus. Nevertheless, outer cylinder rotation devices such as the one used in the present study are valuable because they result in a flow that is more resistant to turbulence. This is because centrifugal instability is avoided and secondary flows are much weaker.<sup>18,19</sup>

Here we study fibrillization using two variants of insulin, human and bovine. Bovine and porcine insulin display similar behavior in humans relative to human insulin and have been used to treat diabetes before recombinant human insulin became widely available.<sup>20,21</sup> Recently there has been renewed interest in animal-derived insulin due to the significant cost of producing recombinant human insulin and the lack of worldwide accessibility.<sup>21</sup> Human and bovine insulin both contain 51 residues and are highly similar in structure. In human insulin, the residues at positions 8 and 10 are threonine (polar) and isoleucine (nonpolar), respectively, while in bovine insulin both residues are valine (nonpolar).<sup>20</sup> The other difference between the two molecules is at position 30, where threonine (polar) in human insulin is replaced by alanine (nonpolar) in bovine insulin.<sup>20</sup>

Mutation of even a single residue within a protein can result in vastly altered fibrillization kinetics.<sup>20,22–24</sup> Under quiescent conditions, bovine insulin typically fibrillizes faster when heated than human insulin.<sup>20,22</sup> A systematic comparison of human and bovine insulin can facilitate investigation of the molecular basis of shear-induced fibrillization, as different proteins should respond differently to shear if the mechanism is related to conformational changes caused by shear. Therefore, the kinetics of bovine and human insulin are compared under uniform shear, and the nucleation and elongation rates are evaluated.

## MATERIALS AND METHODS

**Pretreatment of Insulin.** Both human (91077C) and bovine insulin (I6634) were purchased from Sigma-Aldrich. Because of the sensitivity of fibrillization to seeding and contamination, all glassware was thoroughly cleaned before use. Insulin was dissolved in a solution at pH 1.6 (0.025 M HCl) containing 0.1 M NaCl in deionized water. Once the insulin was dissolved, the solution was cooled to 10 °C before being filtered twice through a 0.2  $\mu\text{m}$  syringe filter. Finally, pH cycling was used to precipitate the insulin and then redissolve it to maximize purity and homogeneity. Filtration combined with pH cycling has been shown to significantly decrease variability between experimental trials.<sup>25,26</sup> All experiments were performed at an insulin concentration of 1 mg/mL after filtration. The fibrillization rate was increased by the use of low pH, high ionic strength, and elevated temperature (65 °C) such that seeding and/or preincubation were not necessary. Mass spectroscopy data for human and bovine insulin processed in this way are given in Figures S11 and S12.

**Turbidity Measurements and Flow Apparatus.** The rotating Couette apparatus used for this experiment is composed of a stationary inner cylinder ( $R_i = 2.22$  cm) and a rotating outer cylinder ( $R_o = 2.5$  cm) constructed from

precision bore borosilicate glass (height  $h = 0.9$  cm). The system was dismantled, and the two cylinders were thoroughly cleaned between each use and recentered for every experiment. A system for in situ detection of amyloid formation from soluble insulin was developed using a 1 mW Helium–Neon laser. The laser is directed through the sample, and laser intensity is recorded with a digital camera at intervals of 10 s. As protein aggregates begin to form, the sample becomes turbid and the laser transmission decreases. The increase in turbidity was shown to correspond to the formation of amyloid fibrils by comparing the laser signal to the increase in fluorescence when using protein tagged by Thioflavin T (See Figure S10). The experimental apparatus (shown in Figure 1) was placed inside an insulated enclosure and heated by a temperature-controlled radiator.

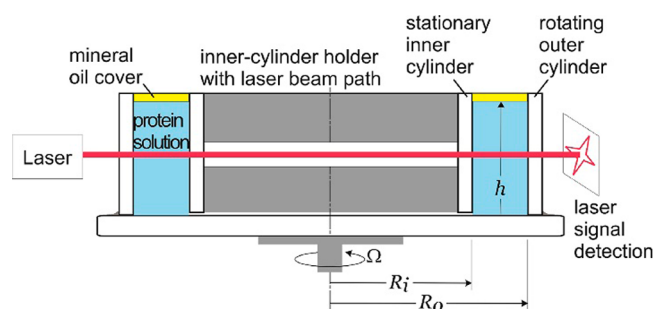


**Figure 1.** Schematic of the flow apparatus consisting of a rotating Couette device and laser probe to detect changes in solution turbidity (not to scale).

It is notable that the formation of amyloid fibrils from bovine insulin is retarded by continuous laser exposure.<sup>27</sup> Because of this effect, control experiments were conducted to test the influence of the laser within the system (Figure S5). This experiment demonstrated that both bovine and human insulin fibrillize slower with laser exposure, but the difference is modest and the effect is similar for both insulin variants. To control for this effect, all experiments were performed with consistent laser exposure.

The insulin solutions placed in the rotating Couette flow system were covered with a layer of mineral oil (Sigma-Aldrich, M5904) for a variety of reasons. First, the aqueous protein solution would evaporate if left open to the environment because the system operates at a high temperature (65 °C). Evaporation would lead to increased protein concentration and influence the fibrillization kinetics in a manner that would be difficult to control.<sup>3</sup> Second, the air–water interface has been shown to have a significant influence on fibrillization kinetics.<sup>15,17</sup> Mineral oil is commonly used to eliminate the air–water interface in biological applications because of the relatively low propensity of proteins to interact with it.<sup>28</sup>

**Microplate Absorbance Measurements.** A BioTek plate reader was used to measure the absorbance of the insulin solutions at 280 nm, and Gen5 Data Analysis software determined the concentration of soluble insulin from sample aliquots. Aliquots of 20  $\mu\text{L}$  were removed from the Couette flow device at specified times throughout the fibrillization experiments and placed in 0.2 mL PCR tubes. The tubes were centrifuged at 6000 rpm for a period of 10 min to remove aggregated protein prior to measurement. Following centrifugation, each time point was measured in duplicate using 4  $\mu\text{L}$  of solution in each well. Control experiments at much higher

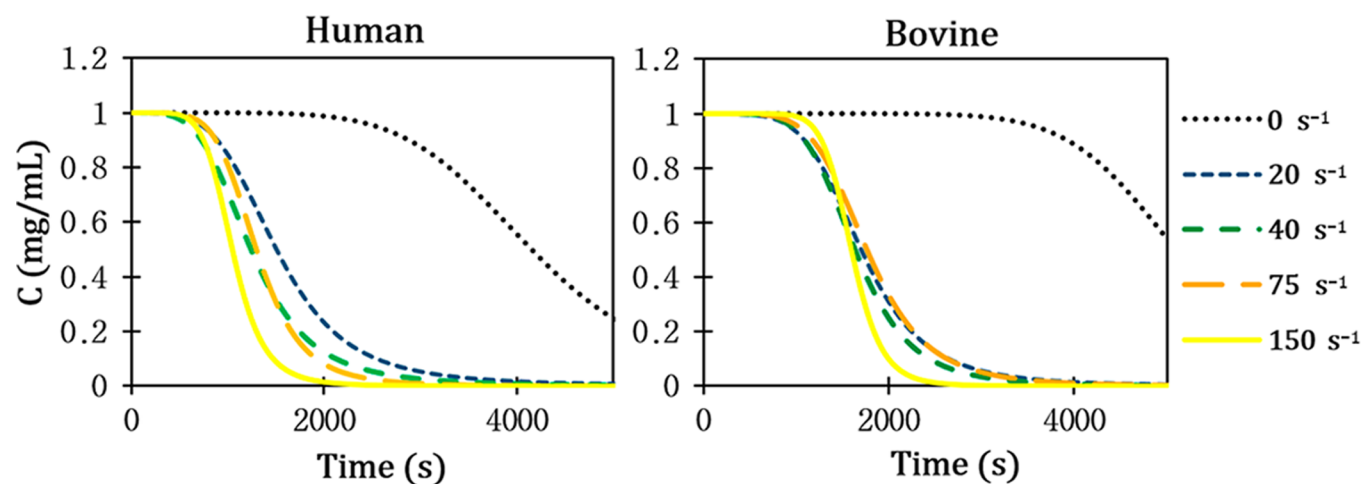


**Figure 2.** Soluble insulin concentration as a function of time for different shear rates measured using the microplate reader. Curves were produced by averaging the sigmoidal parameters of four experiments and then plotting the average fitted curves.

centrifugation speeds demonstrated no changes to the signal (Figure S9).

**Atomic Force Microscopy.** After amyloid fibril assembly was complete, 30  $\mu\text{L}$  of protein solution was deposited onto mica disks (Ted Pella, 50) and protein was allowed to adsorb for a period of 20 min. Samples with adsorbed protein were then rinsed with DI water and left to dry. Samples were sparged with an air stream immediately before imaging to reduce dust accumulation. An AFM (Agilent, MFP3D) was used in tapping mode using cantilever tips with a spring constant of 2 and frequency of 70 kHz (Asylum Research, AC240TS).

**Circular Dichroism Spectroscopy.** Fifty microliter aliquots of solution taken from the Couette flow device were diluted in DI water for a total volume of 300  $\mu\text{L}$ . These samples were then analyzed using a CD Spectrometer (Jasco, 815) at wavelengths of 190 to 260 nm. Relative values for different protein structures could then be determined using the size and position of spectrum peaks in relation to a set of calibration standards for insulin. Representative circular dichroism plots are presented in Figure S4.

**Data Analysis and Parameter Determination.** Two different models were used to study the kinetics of the fibrillization process, a traditional sigmoidal fit and a two-parameter crystallization model. For both models, nonlinear regressions in MATLAB were used to fit time series data to find the best curve fits using data obtained from both the UV measurements and from the turbidity probe. The traditional sigmoidal equation typically used in analyzing fibrillization kinetics is

$$C = \frac{C_0}{1 + \left(\frac{t}{t_{1/2}}\right)^n} \quad (1)$$

where  $C$  is the concentration of monomeric protein,  $C_0$  is the initial concentration, and  $t$  is the time. This equation provides intuitive mathematical parameters for the time at which the signal is at 50% ( $t_{1/2}$ ) and the slope ( $n$ ) of the curve. The kinetics for sigmoidal models are often interpreted using an apparent rate constant, and fibrillization kinetics have been traditionally quantified using such a constant. This rate constant is a function of both the time required for fibrillization and the slope of the curve, and captures the general reaction speed for a

sigmoidal curve better than  $t_{1/2}$  alone. The apparent rate constant was determined as

$$k_{\text{app}} = \frac{2}{t_{1/2} - t_{\text{lag}}} \quad (2)$$

where  $t_{\text{lag}}$  is related to the onset of conformational change and was calculated by finding the maximum slope of the sigmoidal curve and extrapolating to the pretransition base.<sup>29</sup>

The second model used was the two-parameter Finke–Watzky crystallization model, which was originally derived to describe transition-metal nanocluster formation

$$C = \frac{\frac{k_1}{k_2} + C_0}{1 + \frac{k_1}{k_2 C_0} e^{(k_1 + k_2 C_0)t}} \quad (3)$$

where  $k_1$  is the rate constant for nucleation and  $k_2$  is the rate constant for growth. The two independent parameters, nucleation and elongation, make this model useful for determining which steps are most altered by shear. The Finke–Watzky model has proven valuable for accurately describing amyloid fibril kinetic data.<sup>30,31</sup> The assembly of proto-fibrils into fibrils is not captured mathematically by either model, and was instead evaluated using AFM imaging.

**Determination of Mean Shear.** For the concentric cylinder geometry with a rotating outer wall described here, the mean shear rate can be determined as

$$\dot{\gamma} = \frac{2\Omega}{1 + \left(\frac{R_i}{R_o}\right)^2} \quad (4)$$

where  $\dot{\gamma}$  is the mean shear rate,  $\Omega$  is the rotation rate of the outer cylinder in radians per second,  $R_i$  is the radius of the inner cylinder, and  $R_o$  is the radius of the outer. It should be noted that the shear rate presented here is the mean, two-dimensional shear rate while in reality the level of shear in the channel is not perfectly uniform and is dependent on the three-dimensional boundary conditions.

## RESULTS AND DISCUSSION

Measurements of soluble protein obtained via the microplate reader for both human and bovine insulin were performed at six different mean shear rates (0, 20, 40, 75, 110, and 150  $\text{s}^{-1}$ ), with

the results presented in Figure 2. All experiments were repeated four times. The data exhibited typical sigmoidal trends and were analyzed using eq 1. Examples of raw data obtained from both the soluble protein measurements and from the laser turbidity measurements are presented in Figures S1–S3, which also demonstrate the accuracy of both curve-fits.

Figure 2 shows significant difference between the assays in the absence and presence of shear. The difference between the largest ( $150\text{ s}^{-1}$ ) and the smallest shear rates ( $20\text{ s}^{-1}$ ) is small compared to the significant difference between zero shear and the lowest shear rate ( $20\text{ s}^{-1}$ ), a result that has been observed by previous studies.<sup>32</sup> Human insulin is modestly more responsive to different shear levels than bovine insulin. The assays presented in Figure 2 were created from the average parameters of the sigmoidal fit ( $t_{1/2}$  and  $n$ ) from four independent experimental trials.

The laser probe (see Figure 1) was originally incorporated to provide a real-time signal for fibrillization and to reduce the number of experiments that required physical aliquots to be withdrawn and analyzed using the microplate photometer. However, it was discovered that the reduction in the soluble insulin concentration occurred well before the laser transmission was reduced by increased solution turbidity, as seen in Figure 3. This result was unexpected because quiescent experiments have previously demonstrated that the decrease in insulin concentration is well correlated with the increase in fibrillar aggregates (Figure 3, top panel).<sup>3,13</sup> Our results indicate

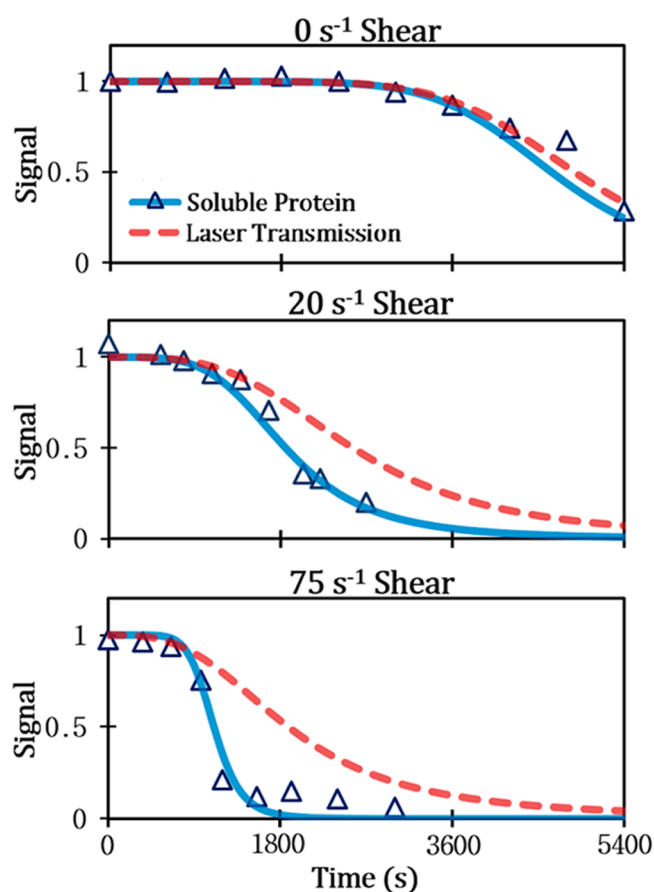


**Figure 3.** Sigmoidal model fits for the normalized turbidity data (detected by laser transmission) and concentration of soluble human insulin (detected by photometry). Discrete points for the soluble insulin concentration are shown.

that imposition of shear alters this behavior. The curves presented in Figure 3 are the sigmoidal fits from discrete experiments (both the laser and soluble data were obtained during the same experiment), as opposed to the average curves presented in Figure 2.

It is notable that the difference between the data for laser transmission and the soluble insulin concentration increases with increasing shear. The laser transmission detects the concentration of fibrils and aggregates that are large enough to result in increased turbidity. The soluble insulin concentration provides an indirect measurement of protein aggregates, as the difference between the initial concentration and the remaining soluble concentration after sedimentation is equal to the concentration of insulin that has aggregated. The difference between the two curves may be attributable to the presence of small, aggregated species that form under shear and are not detected via turbidity measurements. Previous investigations have also found evidence of shear-induced precursor nuclei species that form at the onset of shear but are not present in experiments with heating.<sup>8,17,32</sup> In addition, molecular dynamics simulations have predicted the existence of intermediate species in shear-induced protein unfolding that do not form via other unfolding pathways.<sup>11</sup>

There are modest differences between the overall fibrillization rates of bovine and human insulin as a function of shear. Both molecules respond strongly to the onset of shear, and demonstrate nearly identical  $t_{1/2}$  values at all values of mean shear rate (Figure 4). This result is unexpected, as previous

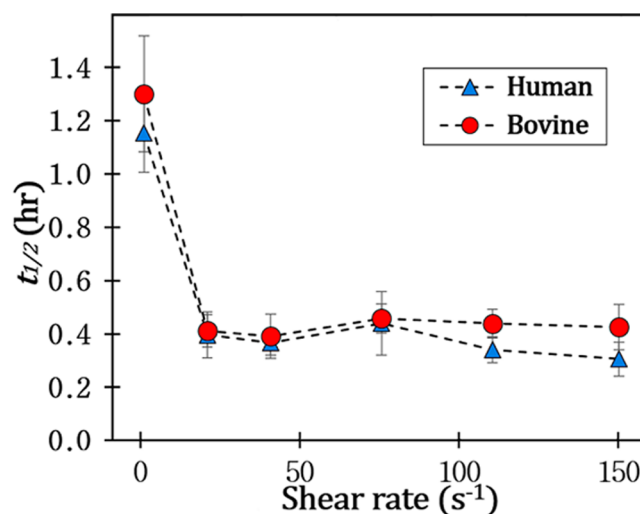


**Figure 4.** Time required to reduce the initial insulin concentration by half ( $t_{1/2}$  from eq 1) as a function of shear rate. Error bars represent standard deviations for four trials.

experiments have concluded that bovine insulin fibrillizes much faster than human insulin under quiescent, heated conditions.<sup>20,22</sup> Indeed, we confirmed the latter result by conducting quiescent control experiments using a heat bath (using the same protein solutions used for the shear experiments). At a constant temperature of  $65\text{ }^{\circ}\text{C}$ , bovine insulin fibrillized approximately three times faster than human insulin (Figure S6). These results suggest bovine insulin fibrillized at nearly the same rate as human insulin within the Couette device for reasons other than simple differences in protein preparation and analysis. Additional control experiments were performed to eliminate uncertainties regarding the effect of the hydrophobic

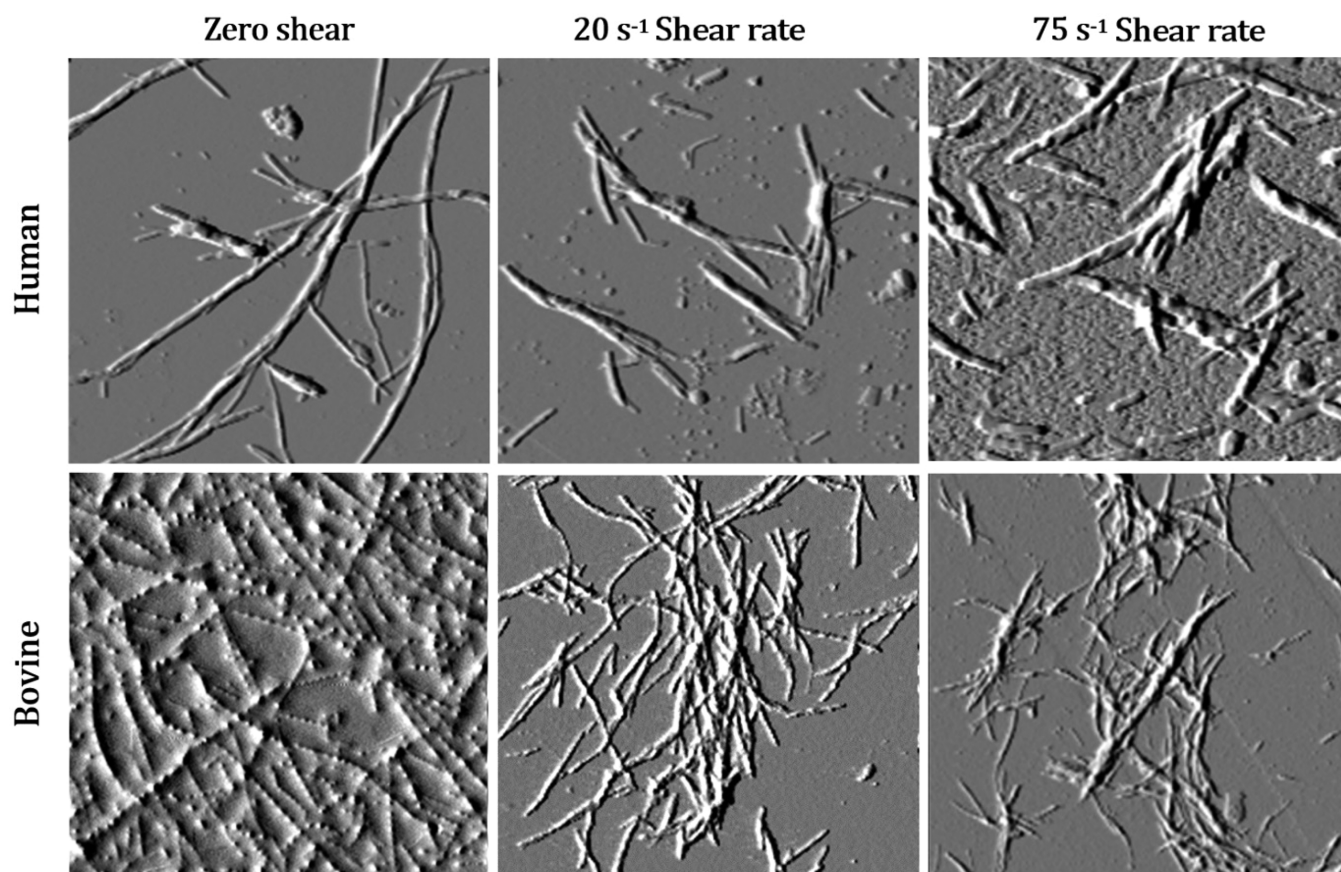


**Figure 5.** AFM images of insulin samples after exposure to different shear rates. The samples were obtained at the end of the shear experiments and deposited on mica. The micrographs are  $3 \times 3 \mu\text{m}$ .

mineral oil interface on fibrillization kinetics, with the conclusion that mineral oil affects human and bovine insulin in similar ways (Figure S7).

AFM images of the aggregates resulting from the shear experiments highlight differences between the shear responses of the human and bovine insulin fibrillization processes (Figure 5). Within the rotating Couette device it was observed that both types of insulin formed fibrils under shear and that the addition of shear resulted in shorter fibrils, a finding that is consistent with previous reports.<sup>6,17</sup> The decreased fibril length may be due to fracturing of the fibrils at high shear rates or to shear-related inhibition of growth from proto-fibrils into mature fibrils.<sup>17</sup> While both types of insulin demonstrated some resistance to forming long fibrils at high shear rates, the physical structures of the two generally differ. Under quiescent conditions, bovine insulin formed fibril-like structures in which individual aggregate “beads” are observed. This suggests that nucleation seeds may have formed first, and the connection of these beads into fibrils occurred later. Numerous AFM images showing these bead-like structures were obtained for bovine insulin under quiescent conditions, while no beads were found in any of the images of human insulin aggregates. A previous report also found that bovine insulin formed nonfibrillar aggregates under low shear and fibrils under high shear within a Couette device.<sup>6</sup> Additional images showing aligned bead aggregates from different quiescent bovine experiments are presented in Figure S8. Under all conditions, bovine insulin fibrils are thinner and rougher than human insulin fibrils.

Fibrillization kinetics of human and bovine insulin were compared by plotting the apparent rate constant (eq 2) against the mean shear rate (Figure 6). This analysis suggests that bovine insulin fibrillizes slightly faster than human insulin. This is due to the bovine insulin assay curves having modestly larger slopes, despite the value of  $t_{1/2}$  being similar for the two insulin variants.

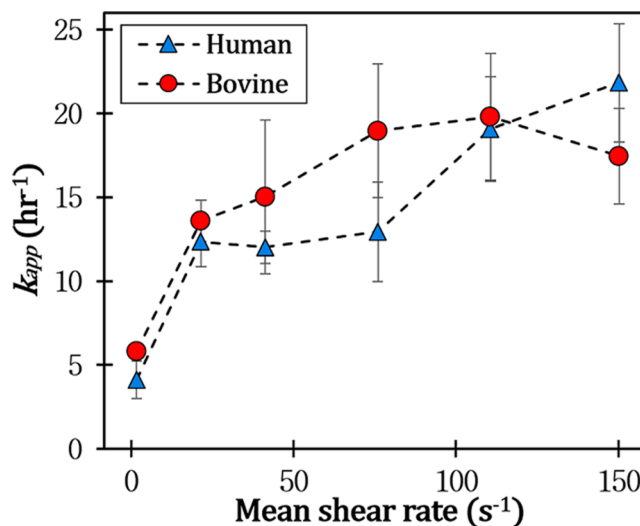


**Figure 6.** Apparent rate constant ( $k_{app}$  from eq 2) for insulin fibrillization as a function of the shear rate. Error bars represent standard deviations for four trials.

Although the apparent rate constant captures the general mathematical trend of the reactions, it fails to capture the actual kinetic rates of discrete steps in amyloid formation. For a more detailed analysis, the Finke–Watzky crystallization model eq 3 was used to separate the nucleation and elongation steps. Figure 7 compares the nucleation constant  $k_1$  for human and

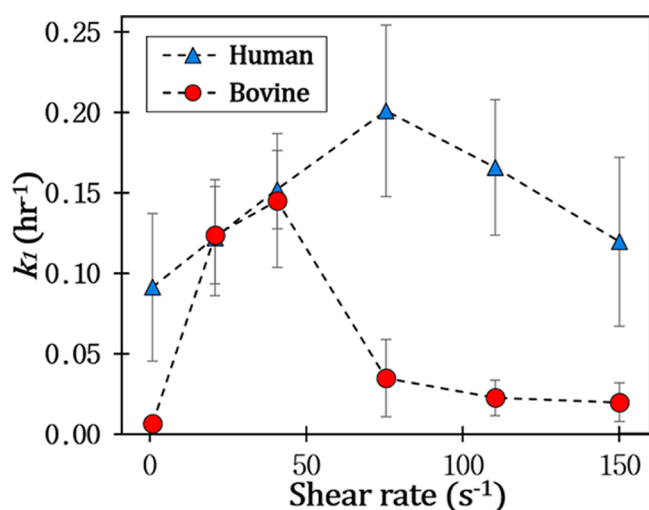


**Figure 7.** Nucleation rate constant for human and bovine insulin fibrillization ( $k_1$  from Finke–Watzky model, eq 3). Error bars are standard deviations for four replicates.

bovine insulin obtained from a regression fit of the data. Interestingly, there appears to be a peak value of the nucleation rate constant at intermediate shear rates for both human and bovine insulin. This peak indicates that shear above a critical value inhibits nucleation. Previous work has demonstrated that there is a minimum fibrillization time ( $t_{1/2}$ ) at intermediate values of shear for apolipoprotein-C,<sup>7</sup> and that whey protein has a peak fibrillization rate at intermediate values of shear.<sup>33</sup> This suggests that a critical shear rate for maximum nucleation occurs for different types of proteins.

An analog to this observation was recently reported in which pressure-jump kinetics of protein folding and unfolding were investigated.<sup>34</sup> It was determined that there exists an intermediate pressure where neither folding nor unfolding rates dominate and the value of the inverse sum of the two rates has a maximum peak. The position and size of the peak depended on the protein structure, and specifically on the volume of internal cavities within the protein. Similarly, many nucleation-dependent crystallization reactions are known to exhibit a peak rate at intermediate temperatures.<sup>35–37</sup>

It is possible that the primary effect of shear on nucleation is to increase the number and energetics of molecular interactions between insulin monomers. Increasing shear allows more successful reactions to occur until a point at which molecules are moving too fast for collisions to successfully result in reaction and nucleation. Previous reports have posited that shear increases polymerization of nuclei at low shear rates, but at higher shear rates the extensional component of the flow overwhelms the strength of the hydrogen bonds required to stabilize aggregating nuclei.<sup>17,33</sup>

The nucleation rate constant for human and bovine insulin exhibit different peak values, and the difference between the two is particularly notable at  $75 s^{-1}$ . Figure S4 gives the circular dichroism analysis of experiments conducted at  $75 s^{-1}$ . It is

interesting to note that the human insulin spectrograph shows only small losses in  $\alpha$  helix structure for the first 16 min, but by the time the 20 min sample was taken the  $\alpha$  helix structure had decreased significantly, giving way to  $\beta$  sheet structures. This same large drop was not observed for the bovine insulin at  $75 s^{-1}$ . It is likely that this difference is related to the nucleation rate constant, as a faster nucleation rate results in a much faster transition between soluble and fibrillized protein.

The second parameter of the Finke–Watzky model is the elongation rate constant,  $k_2$ , plotted in Figure 8. The elongation

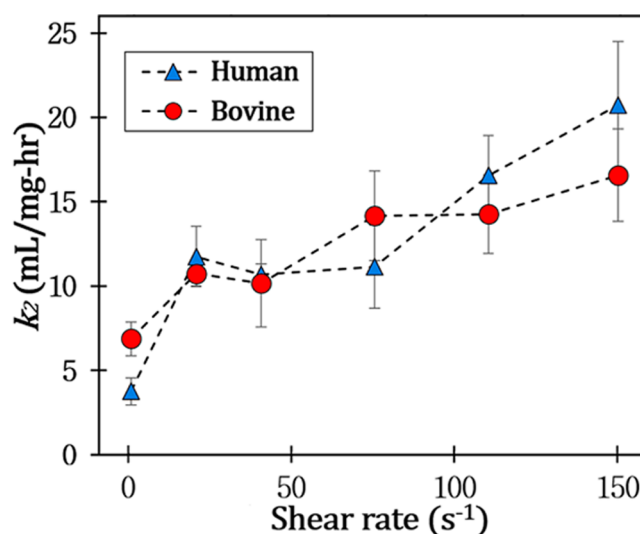


**Figure 8.** Elongation rate for insulin fibrillization as a function of shear rate ( $k_2$  of Finke–Watzky model, eq 3). Error bars are standard deviations for four replicates.

constant refers to the rate that native monomers are removed from solution following nucleation. At higher shear rates the effect of mixing in solution will be more pronounced because of the increased velocity gradient. Because human and bovine insulin have similar rate constants when exposed to the same flow field, it can be inferred that this constant is better correlated to the effect of mixing than it is to the effects of shear on the molecules themselves. This is contrasted to nucleation where higher velocity gradients do not correspond to an increased rate. It can be observed that the compensatory effects of the two Finke–Watzky rate constants combine in a way that recovers  $k_{app}$ .

Unfolding and aggregation of protein has been demonstrated to be vastly increased by flow here and in many previous studies. However, the mechanism for this kinetic increase is unclear. The theory that shear-induced extensional force results in breaking of the tertiary structure hydrogen bonds is supported by observations of large polymeric proteins under shear fields. For example, the effect of shear on multimeric human von Willebrand Factor (VWF) is thought to be responsible for clotting behavior of blood at the site of an injury. It has been found that shear forces are able to disrupt domain interactions and induce stretching of the VWF molecule, leading to conformational changes and aggregation.<sup>38,39</sup> However, it is not possible to apply this hypothesis to smaller molecules because the force required to break the hydrogen bonds of proteins is far too great to have been imposed by shear. VWF multimers range between 500 and 20 000 kDa in size, while insulin is only 5 kDa and unlikely to

experience the extensional strain required for conformational change. Other theories predict that alignment of monomers within a shear field results in fibril formation. However, it can be argued that proteins on the order of 5 kDa are essentially isotropic and too small for significant alignment to occur. Flow-induced alignment may play a role in elongation but not in nucleation.

## CONCLUSIONS

The observed nonmonotonic effect of shear on the nucleation rate of insulin aggregation is novel. Previous studies<sup>7,33</sup> had reported peak fibrillization rates at intermediate shear but the present results are the first to demonstrate that nucleation is the mechanism responsible for this observation. It is clear that nucleation is not a simple function of increased shear, but rather is dependent on the energetics of molecular interactions. These results suggest that shear-induced mixing is an important mechanism that may have been underestimated by previous reports. It should be noted that a previous investigation asserted that the effect of agitation on fibrillization was not due to increased mixing and mass transfer, but was instead due to effects of hydrophobic interfaces in conjunction with agitation.<sup>15</sup> Only a small proportion of the interface was hydrophobic in the present experiments, but it may have played a role in fibrillization. However, the fact that a peak nucleation rate was observed at intermediate shear levels with a fixed hydrophobic proportion suggests that interfacial effects alone do not fully explain shear-induced fibrillization.

While many fibrillization studies report kinetics in terms of the apparent rate constant or via the raw data that comprises fibrillization assays, there is opportunity to further probe molecular mechanisms via kinetic models. The Finke–Watzky model proved useful in isolating the effect of shear on the separate stages of fibrillization. The compensatory behavior of the nucleation and elongation rate constants effectively demonstrates that while apparent rate constants can be useful for making general statements about fibrillization kinetics, the individual steps should be considered separately to ascertain sufficient information about the process.

The lag between the curves showing the decrease in soluble insulin concentration and the increase in turbidity (Figure 3) necessitates caution in interpretation of data when using turbidity methods to detect aggregates under flowing conditions. The variation of the observed lag with shear rate suggests the existence of small aggregates that are created by shear. These intermediate species are likely related to the differences observed between quiescent and shear-induced fibrillization rates and mechanisms, particularly in regard to nucleation pathways.

## ASSOCIATED CONTENT

### Supporting Information

The Supporting Information is available free of charge on the ACS Publications website at DOI: 10.1021/acs.jpbc.5b04488.

Summary of data plotted in the main body, example plots of raw data to demonstrate goodness-of-fit to the models, circular dichroism plots, control results for the effect of laser exposure on fibrillization kinetics and the influence of mineral oil, assays obtained from heat bath experiments, AFM images of bovine aggregates at zero shear, control experiments testing validity of experimental

methods, and mass spectroscopy data for the insulin solutions. (PDF)

## AUTHOR INFORMATION

### Corresponding Author

\*E-mail: [hirsaa@rpi.edu](mailto:hirsaa@rpi.edu). Tel: (518) 276-6997.

### Author Contributions

S.A.M. developed and performed the experiments and wrote the first draft of the manuscript, C.F.T. designed and constructed the flow apparatus and turbidity probe and assisted in the early experiments, S.P.S. performed many of the repeated trials of the experiments, P.M.T. assisted with data interpretation and editing the manuscript, and A.H.H. developed the experiment concept and served as research adviser to S.A.M., C.F.T., and S.P.S., and assisted with the manuscript.

### Notes

The authors declare no competing financial interest.

## ACKNOWLEDGMENTS

S.A.M., C.F.T., and A.H.H. thank NASA for their support under grant NNX13AQ22G. We thank Juan M. Lopez for insights on the rotating Couette flow apparatus. We also thank Dmitri Zagorevski for providing the mass spectrometry data showing purity of the insulin solutions.

## REFERENCES

- (1) Alzheimer, A. Über eine eigenartige Erkrankung der Hirnrinde. *Allgemeine Zeitschrift für Psychiatrie und phychisch-Gerichtliche Medizin* **1907**, *64* (1–2), 146–148.
- (2) Chiti, F.; Dobson, C. M. Protein Misfolding, Functional Amyloid, and Human Disease. *Annu. Rev. Biochem.* **2006**, *75*, 333–66.
- (3) Nielsen, L.; Khurana, R.; Coats, A.; Frokjaer, S.; Brange, J.; Vyas, S.; Uversky, V. N.; Fink, A. L. Effect of Environmental Factors on the Kinetics of Insulin Fibril Formation: Elucidation of the Molecular Mechanism. *Biochemistry* **2001**, *40*, 6036–6046.
- (4) Sluzky, V.; Tamada, J. A.; Klivanov, A. M.; Langer, R. Kinetics of Insulin Aggregation in Aqueous Solutions upon Agitation in the Presence of Hydrophobic Surfaces. *Proc. Natl. Acad. Sci. U. S. A.* **1991**, *88* (21), 9377–9381.
- (5) Hamilton-Brown, P.; Bekard, I. B.; Ducker, W. A.; Dunstan, D. A. How does Shear Affect Amyloid Beta Fibrillogenesis? *J. Phys. Chem. B* **2008**, *112*, 16249–16252.
- (6) Bekard, I. B.; Dunstan, D. E. Shear-induced Deformation of Bovine Insulin in Couette Flow. *J. Phys. Chem. B* **2009**, *113*, 8453–8457.
- (7) Teoh, C. L.; Bekard, I. B.; Asimakis, P.; Griffin, M. D. W.; Ryan, T. M.; Dunstan, D. E.; Howlett, G. J. Shear Flow Induced Changes in Apolipoprotein C-II Conformation and Amyloid Fibril Formation. *Biochemistry* **2011**, *50*, 4046–4057.
- (8) Hill, E. K.; Krebs, B.; Goodall, D. G.; Howlett, G. J.; Dunstan, D. E. Shear Flow Induces Amyloid Fibril Formation. *Biomacromolecules* **2006**, *7*, 10–13.
- (9) Dunstan, D. E.; Hamilton-Brown, P.; Asimakis, P.; Ducker, W.; Bertolini, J. Shear-induced Structure and Mechanics of Beta-Lactoglobulin Amyloid Fibrils. *Soft Matter* **2009**, *5*, 5020–5028.
- (10) Chateaneuf, G. M.; Mikulski, P. T.; Gao, G. T.; Harrison, J. A. Compression and Shear Induced Polymerization in Model Diactylene-Containing Monolayers. *J. Phys. Chem. B* **2004**, *108*, 16626–16635.
- (11) Szymczak, P.; Cieplak, M. Proteins in a Shear Flow. *J. Chem. Phys.* **2007**, *127* (15), 155106.
- (12) Jaspe, J.; Hagen, S. J. Do Protein Molecules Unfold in a Simple Shear Flow? *Biophys. J.* **2006**, *91*, 3415–3424.

- (13) Lee, C. C.; Nayak, A.; Sethuraman, A.; Belfort, G.; McRae, G. J. A Three-stage Kinetic Model of Amyloid Fibrillation. *Biophys. J.* **2007**, *92*, 3448–3458.
- (14) Dunstan, D. E.; Hamilton-Brown, P.; Asimakis, P.; Ducker, W.; Bertolini, J. Shear Flow Promotes Amyloid-Beta Fibrillation. *Protein Eng., Des. Sel.* **2009**, *22* (12), 741–746.
- (15) Pronchik, J.; He, X.; Giurleo, J. T.; Talaga, D. S. In Vitro Formation of Amyloid from Alpha-Synuclein is Dominated by Reaction at Hydrophobic Interfaces. *J. Am. Chem. Soc.* **2010**, *132*, 9797–9803.
- (16) Ashton, L.; Dusting, J.; Imomoh, E.; Balabani, S.; Blanch, E. W. Shear-Induced Unfolding of Lysozyme Monitored In Situ. *Biophys. J.* **2009**, *96*, 4231–4236.
- (17) Bekard, I. B.; Asimakis, A.; Bertolini, J.; Dunstan, D. E. The Effects of Shear Flow on Protein Structure and Function: Review. *Biopolymers* **2011**, *95* (11), 733–746.
- (18) Drazin, P. G.; Reid, W. H. *Hydrodynamic Stability*; Cambridge University Press: Cambridge, U.K., 1981. DOI: [10.1017/CBO9780511616938](https://doi.org/10.1017/CBO9780511616938).
- (19) Schulz, A.; Pfister, G.; Tavener, S. J. The Effect of Outer Cylinder Rotation on Taylor-Couette Flow at Small Aspect Ratio. *Phys. Fluids* **2003**, *15* (2), 417–425.
- (20) Nielsen, L.; Frokjaer, S.; Brange, J.; Uversky, V. N.; Fink, A. L. Probing the Mechanism of Insulin Fibril Formation with Insulin Mutants. *Biochemistry* **2001**, *40*, 8397–8409.
- (21) Greene, J. A.; Riggs, K. R. Why is there no Generic Insulin? Historical Origins of a Modern Problem. *N. Engl. J. Med.* **2015**, *372*, 1171–1175.
- (22) Morales, P. B. Kinetics of Human and Bovine Insulin Amyloid Fibril Formation in the Presence of Solid/liquid Interfaces. M.S. thesis, Missouri University of Science and Technology, 2013.
- (23) Oliva, A.; Santovena, A.; Farina, J.; Llabres, M. Effect of High Shear Rate on Stability of Proteins: Kinetic Study. *J. Pharm. Biomed. Anal.* **2003**, *33*, 145–155.
- (24) Meisl, G.; Yang, X.; Hellstrand, E.; Forhm, B.; Kirkegaard, J. B.; Cohen, S. I. A.; Dobsen, C. M.; Linse, S.; Knowles, T. P. J. Differences in Nucleation Behavior Underlie the Contrasting Aggregation Kinetics of the AB40 and AB42 Peptides. *Proc. Natl. Acad. Sci. U. S. A.* **2014**, *111* (26), 9384–9389.
- (25) Teplow, D. B. Preparation of Amyloid Beta-Protein for Structural and Functional Studies. *Methods Enzymol.* **2006**, *413*, 20–30.
- (26) Posada, D.; Tessier, P. M.; Hirs, A. H. Removal versus Fragmentation of Amyloid Fibril Precursors via Membrane Filtration. *Biotechnol. Bioeng.* **2012**, *109* (3), 840–845.
- (27) Liu, R.; Su, R.; Qi, W.; He, Z. Photo-induced Inhibition of Insulin Amyloid Fibrillation on Online Laser Measurement. *Biochem. Biophys. Res. Commun.* **2011**, *409* (2), 229–234.
- (28) Shimura, K.; Uchiyama, N.; Kasai, K. Prevention of Evaporation of Small-Volume Sample Solutions for Capillary Electrophoresis using a Mineral-oil Overlay. *Electrophoresis* **2001**, *22* (16), 2471–2477.
- (29) Arosio, P.; Knowles, T. P. J.; Linse, S. On the Lag Phase in Amyloid Fibril Formation. *Phys. Chem. Chem. Phys.* **2015**, *17*, 7606–7618.
- (30) Morris, A. M.; Watzky, M. A.; Finke, R. G. Protein Aggregation Kinetics, Mechanism, and Curve-fitting: A Review of the Literature. *Biochim. Biophys. Acta, Proteins Proteomics* **2009**, *1794*, 375–397.
- (31) Crespo, R.; Rocha, F. A.; Ana, M. A Generic Crystallization-like Model that Describes the Kinetics of Amyloid Fibril Formation. *J. Biol. Chem.* **2012**, *287*, 30585–30594.
- (32) Akkermans, C.; Venema, P.; Rogers, S. S.; van der Goot, A.; Boom, R. M.; van der Linden, E. Shear Pulses Nucleate Fibril Formation. *Food Biophys.* **2006**, *1*, 144–150.
- (33) Akkermans, C.; van der Goot, A. J.; Venema, P.; van der Linden, E.; Boom, R. M. Formation of Fibrillar Whey Protein Aggregates: Influence of Heat and Shear Treatment, and Resulting Rheology. *Food Hydrocolloids* **2008**, *22*, 1315–1325.
- (34) Roche, J.; Dellarole, M.; Caro, J. A.; Norberto, D. R.; Garcia, A. E.; Garco-Moreno, B.; Roumestand, C.; Royer, C. A. Effect of Internal Cavities on Folding Rates and Routes Revealed by Real-Time Pressure Jump NMR Spectroscopy. *J. Am. Chem. Soc.* **2013**, *135*, 14610–14618.
- (35) Galkin, O.; Vekilov, P. G. Nucleation of Protein Crystals: Critical Nuclei, Phase Behavior, and Control Pathways. *J. Cryst. Growth* **2001**, *232* (1–4), 63–76.
- (36) Perepezko, J. H. Nucleation-Controlled Reactions and Metastable Structures. *Prog. Mater. Sci.* **2004**, *49*, 263–284.
- (37) Gunton, J. D.; Shirayev, A.; Pagan, D. L. *Protein Condensation: Kinetic Pathways to Crystallization and Disease*; Cambridge University Press: Cambridge, U.K., 2007.
- (38) Singh, I.; Themistou, E.; Porcar, L.; Neelamegham, S. Fluid Shear Induces Conformation Change in Human Blood Protein von Willebrand Factor in Solution. *Biophys. J.* **2009**, *96*, 2313–2320.
- (39) Di Stasio, E.; De Cristofaro, R. The Effect of Shear Stress on Protein Conformation: Physical Forces Operating on Biological Systems: The Case of the Von Willebrand Factor. *Biophys. Chem.* **2010**, *153* (1), 1–8.